# Inorganic Chemistry Cite This: Inorg. Chem. 2019, 58, 8339–8346

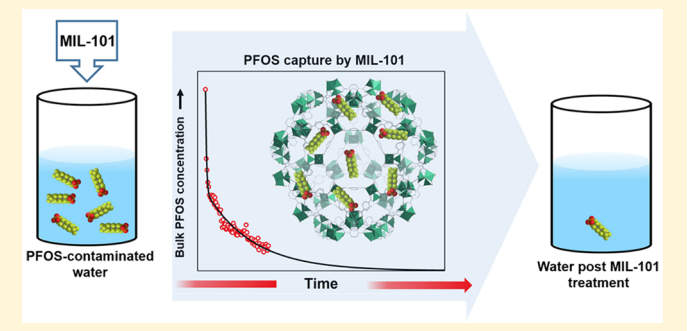
pubs.acs.org/IC

# Probing the Sorption of Perfluorooctanesulfonate Using Mesoporous Metal-Organic Frameworks from Agueous Solutions

Dushyant Barpaga, † Dian Zheng, \* Kee Sung Han, † Jennifer A. Soltis, † Vaithiyalingam Shutthanandan, Sagnik Basuray, B. Peter McGrail, Sayandev Chatterjee, \* Jennifer A. Soltis, Sayandev Chatterje and Radha Kishan Motkuri\*,†®

Supporting Information

ABSTRACT: One approach to reduce increasing concentrations of toxic per- and polyfluoroalkyl substances (PFAS) involves the capture of PFAS from aqueous media using porous materials. The use of highly porous, tunable metal organic framework (MOF) materials is appealing for targeted liquid phase sorption. In this work, we demonstrate the excellent capture of perfluorooctanesulfonate (PFOS) using both the chromium and iron analogs of the MIL-101 framework. Experimental characterization of PFOS uptake reveals unique differences in sorption properties between these two analogs, providing key implications for future PFOS sorbent design. Specifically, STEM-EDS and IR spectroscopy



show definitive proof of sorption. Furthermore, XPS analysis shows evidence of a strong interaction between sulfur atoms of the polar headgroup of PFOS and the metal center of the framework in addition to the fluorinated nonpolar tail. Additionally, in situ <sup>19</sup>F NMR reveals higher PFOS affinity for Cr-MIL-101 versus Fe-MIL-101 based on sorption kinetics. Surprisingly, at these relatively high PFOS concentrations, activated acetylene black carbon is severely outperformed by both MOFs.

# ■ INTRODUCTION

Toxic per- and polyfluoroalkyl substances (PFAS) are known to be released into the environment from a number of anthropogenic sources. Given their high chemical resistance and thermal stabilities, these surfactants are routinely used in applications for the semiconductor and photolithography industries and found in fire extinguishers, firefighting foams, and fabric protectors. 1,2 Unfortunately, their low volatility, high water solubility, and extreme resistance to degradation have made them ubiquitous in the environment. Continued regular usage of these technologies has increased PFAS concentrations in contaminated sites to several orders of magnitude higher than the US EPA health advisory level (HAL) for drinking water. Their toxicity and persistence in the human body targets blood and organs such as the liver, causing many health problems that have been linked to disease and cancers.5-Therefore, although the elimination of such substances directly from its sourced application is necessary, the decrease in accumulated human consumption of PFAS is of primary concern.

To combat increasing concentrations of PFAS in drinking water, several approaches have been developed, including photocatalysis, biological degradation and sonolysis; however, these technologies suffer from inherent weaknesses such as inefficiency, high energy consumption, and the need for specialized equipment.  $^{8-10}$  On the other hand, sorption methodology has proven to be an effective and cost-efficient process. Promising candidate materials must include high affinity for PFAS, fast uptake rates, and large overall capacities. Use of traditional adsorbents such as activated carbons, carbon nanotubes, and ion-exchange resins have shown successful removal of these contaminants even though significant potential for engineered porous materials remains. 11-14 To this end, recently prolific materials, metal-organic frameworks (MOFs), have gained substantial attention mainly because of their very high surface areas, high pore volumes, and versatile functionalities. More importantly, their modular synthesis allows tunability toward targeted sorbates, which has led to extensive research in applications such as sorption,  $^{15-18}$  separation,  $^{19-23}$  catalysis,  $^{24-26}$  and sensing.  $^{27-29}$  The design materials for targeted recognition of environmental

Received: February 8, 2019 Published: May 8, 2019



8339

<sup>&</sup>lt;sup>†</sup>Energy and Environment Directorate, Pacific Northwest National Laboratory, Richland, Washington 99352, United States <sup>‡</sup>Physical and Computational Sciences Directorate, Pacific Northwest National Laboratory, Richland, Washington 99352, United States

<sup>§</sup>Earth and Biological Sciences Directorate, Pacific Northwest National Laboratory, Richland, Washington 99352, United States Department of Chemical and Materials Engineering, New Jersey Institute of Technology, Newark, New Jersey 07102, United States

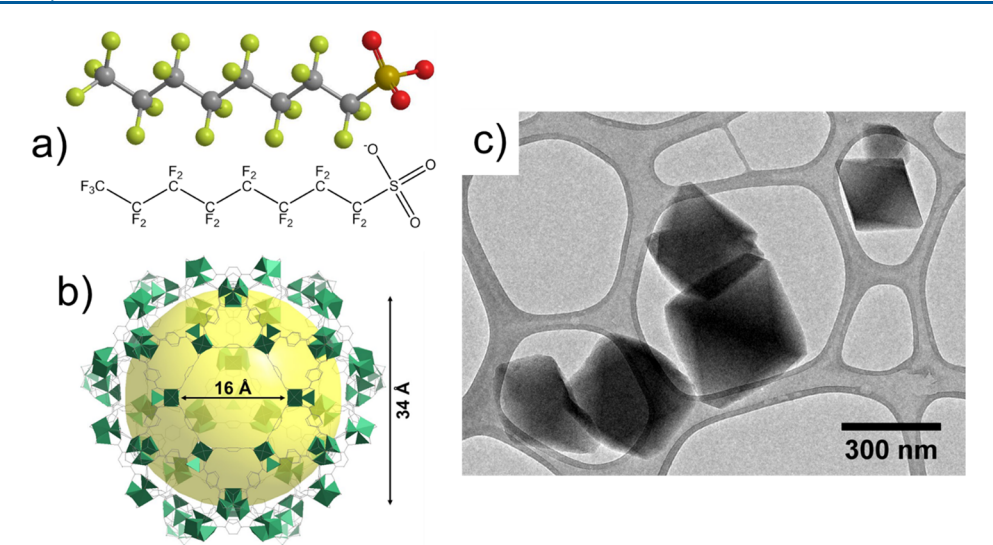


Figure 1. (a) Structure of a perfluorooctanesulfonate anion. (b) Mesoporous cage of the MIL-101 framework. (c) Representative transmission electron microscope image of Cr-MIL-101 particles.

contaminants has been one of the key challenges in environmental chemistry; 30-33 these materials fall into this category and can be synergized with established approaches for their rapid and sensitive detection using chemical or electrochemical methods. 34,35

Limited studies have reported the use of MOFs to capture PFAS. Sini et al. utilized zirconium-based UiO-66 to show enhanced affinity for perfluorooctanesulfonate (PFOS) and perfluorooctanoate anions using fluorinated functionalities in the pore that promote fluorine-fluorine interactions.<sup>36</sup> Liu et al. utilized Cr(III) terephthalate, Cr-MIL-101, which adsorbed a promising amount of perfluorooctanoic acid (PFOA) due to its high surface area and large pore volume.<sup>37</sup> Chen et al. utilized similar ZIF materials, ZIF-7, ZIF-8, and ZIF-L, to probe PFOA sorption behavior as a function of structural topology and surface functionality, finding that interlayer spacing from a layered structure leads to higher uptake.<sup>38</sup> Li et al. utilized a mesoporous cationic thorium-based SCU-8 to study the dynamics of PFOS uptake via molecular simulations that reveal multiple driving forces of sorption.<sup>39</sup> Key elements from these studies include the necessity of a sorbent material with large pores for high diffusivity, fast kinetics, and greater accessibility of target PFAS molecules to strong sorption sites like surface functionalities and metal centers. In general, PFAS sorption relies on both hydrophobic and electrostatic interactions.<sup>8,38</sup> The hydrophobicity of the perfluoroalkyl tail increases with increasing chain length and the presence of more C-F bonds. The pH of sorption media, affected by the sample matrix or the adsorbent itself, can influence changes in electrostatic interactions between PFAS and the sorbent. These factors influencing the sorption mechanism must be considered when identifying suitable potential adsorbent materials. Therefore, we aim to further the understanding of PFAS sorption by studying its capture on similar MOF

Among the most prominent PFAS contaminants found in aqueous environments, PFOS (Figure 1a) has proven to be physiologically persistent and stable and has been linked to numerous health issues upon prolonged, cumulative exposure. To this end, for the purpose of this study, MOF frameworks were probed with PFOS. Although PFAS detection limits for

novel sensor materials now have now dropped to far lower than 1 ppm, our goal was to test concentrations near saturation to observe capture potential with MOF candidates using relatively greater PFAS concentrations so that their uptake performance can be compared with traditional carbon sorbents in widespread use in industry and government. 40,41

Deriving motivation from these studies and our recent success in finding promising fluorocarbon sorbent materials, 42-44 here we considered the role of metal cations in mesoporous MIL-101 framework family, namely Cr-MIL-101 and Fe-MIL-101, to adsorb PFOS. 45 MIL-101, originally developed by Ferey et al., consists of  $M^{+3}$  (where M = Cr or Fe) nodes linked by 1,4-benzene dicarboxylate (BDC) to form mesoporous cages of  $\sim$ 29 and 34 Å as shown in Figure 1b.  $^{46,47}$ The high surface area, pore volume, unsaturated sorption sites, and stability of MIL-101 make it very appealing for sorbate capture. These superior sorbent characteristics, in addition to the role of the metal node, were probed in this study for PFOS sorption in comparison with a commercial carbon material, acetylene black granular activated carbon (GAC), a well-used sorbent for PFAS removal at United States Department of Defense sites. We utilize <sup>19</sup>F nuclear magnetic resonance (NMR) to characterize the uptake and capture of PFOS from high concentration aqueous solutions using Cr-MIL-101, Fe-MIL-101, and activated carbon. We also utilize infrared (IR) and X-ray photoelectron spectroscopy (XPS) methods to analyze the presence and nature of PFOS sorption on both MIL-101 MOFs.

#### EXPERIMENTAL METHODS

**MOF Synthesis.** Cr-MIL-101 was synthesized under hydrothermal conditions as previously reported in the literature. Briefly, in a Parr reactor liner, chromium(III) nitrate nonahydrate (Cr-(NO<sub>3</sub>)<sub>3</sub>·9H<sub>2</sub>O, 8.4 mmol) and terephthalic acid (BDC, 8.4 mmol) were added to distilled water (40 mL) and stirred vigorously for 30 min. The liner was sealed in the vessel and placed in an oven at 200 °C for 24 h. After cooling to room temperature, the contents of the as-synthesized product was centrifuged and washed with water (3 × 30 mL) repeatedly. To further isolate the MOF, the filtered product was washed with  $N_iN$ -dimethylformamide (3 × 30 mL) repeatedly over the course of 24 h. Finally, the solvent was exchanged with methanol (3 × 30 mL) over the course of another 24 h. The product

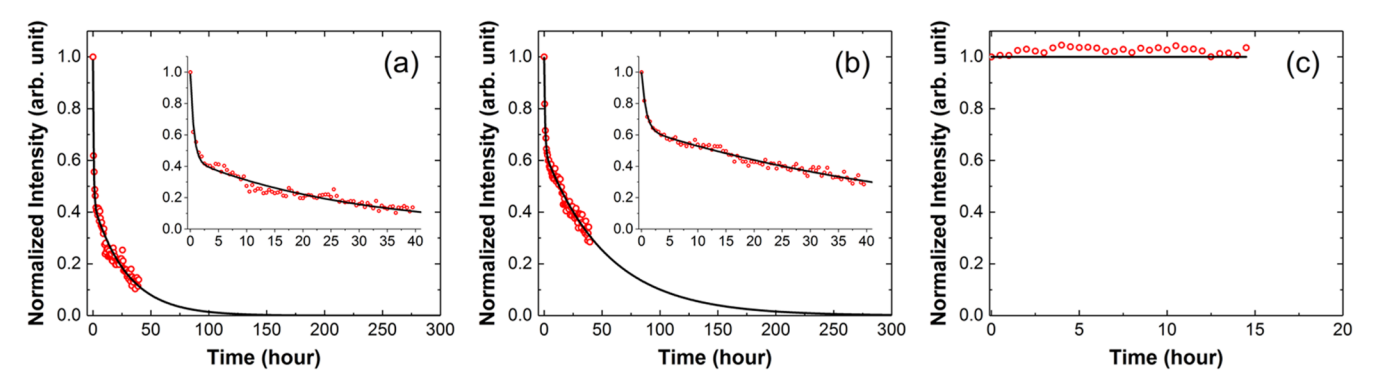


Figure 2. Normalized intensities (area) of the  $^{19}$ F NMR peak centered at -79 ppm (O) tracked over time upon addition of 800  $\mu$ L of 10 mM PFOS/H<sub>2</sub>O to (a) Cr-MIL-101 (8.6 mg), (b) Fe-MIL-101 (8.2 mg), and (c) granular activated carbon (9.4 mg). Red circles represent collected data while black lines represent fitted curves. Insets show data and corresponding fits for the first 40 h of data collection.

was dried in a vacuum oven at 70  $^{\circ}$ C overnight and activated at 150  $^{\circ}$ C for 24 h prior to characterization.

Fe-MIL-101 was synthesized similar to as previously reported in the literature. Briefly, in a Parr reactor liner, iron(III) chloride hexahydrate (FeCl $_3$ ·GH $_2$ O, 4 mmol), terephthalic acid (BDC, 4 mmol), and acetic acid (2 mL) were added to N,N-dimethylformamide (50 mL) and stirred vigorously for 30 min. The liner was sealed in the vessel and placed in an oven at 120 °C for 24 h. After cooling to room temperature, the contents of the as-synthesized product was centrifuged and washed with fresh N,N-dimethylformamide (3 × 30 mL) repeatedly. Finally, the solvent was exchanged with methanol (3 × 30 mL) over the course of another 24 h. The product was dried in a vacuum oven at 70 °C overnight and activated at 150 °C for 24 h prior to characterization.

PFOS Exposure. Concentrated PFOS (Sigma-Aldrich) was diluted in DI water to concentrations of 100, 50, 10, and 1 mM solutions. Preliminary tests with <sup>19</sup>F NMR revealed that the time scale for full sorption using 1 mM solutions was on the order of seconds, while for 100 mM solutions, it was on the order of days (Figure S1). To collect a reasonable amount of data points per experiment, known volumes of 10 mM solutions (~1 mL) were added to a consistent amount of sorbent material (~10 mg) to obtain data on a time scale of several hours. For this reason, aliquots of a stock solution of 10 mM PFOS were utilized to prepare samples for all experimental characterization methods. To expose sorbents with PFOS, presynthesized and activated (at 150 °C for 24 h under vacuum) materials were soaked in an aqueous solution of PFOS (10 mM) under stirring for 24 h. The mixture was allowed to soak for another 24 h without stirring. Finally, the water was removed by heating the solution to 100 °C in a convection oven for 24 h. Once dried, the recovered product was activated again under vacuum at 150 °C for 24 h prior to characterization. Dried samples were denoted as [PFOS]-M-MIL-101 (where M = Cr or Fe).

Post Sorption Characterization. Liquid-state <sup>19</sup>F NMR measurements were performed on a 10 mM PFOS solution (~1 mL) before, during, or after contact with ~10 mg of sorbent material. Experiments were conducted using a 750 MHz NMR spectrometer (Agilent, USA) with a 5 mm wideband HXY probe at room temperature as a function of time and continued up to ~40 h with the time interval of 30 min. 19F NMR spectra were accumulated on the Larmor frequency of 705.83 MHz using a single pulse excitation. The solid-state <sup>19</sup>F NMR was performed on the material that was exposed to PFOS solution in the 19F solution NMR experiments; the solids were separated and dried in a convection oven at 120 °C for 24 h. The spectra were accumulated with a 4 mm HFXY magic angle spinning (MAS) probe on a 600 MHz solid-state NMR spectrometer (Agilent, USA) on the Larmor frequency of 564.68 MHz using a spin-echo sequence at spinning speed of 14 kHz. The <sup>19</sup>F chemical shift for both liquid- and solid-state experiments was calibrated against pure CF<sub>3</sub>CH<sub>2</sub>OH (-78 ppm) as external reference. For the samples containing PFOS, the resonance at -79 ppm, which showed a high

baseline and high intensity as compared to other fluorine resonances, was utilized to measure sorption kinetics.

IR measurements were collected on both parent MOFs materials as well as post PFOS exposure using a ThermoScientific Nicolet FTIR spectrometer equipped with  ${\rm CaF_2}$  windows and an MCT detector with a resolution of 4 cm $^{-1}$ . A minimum of 64 scans were accumulated for each spectrum. The solid MOF materials were mixed with KBr powder to form pellets before characterization. The spectrum for pure KBr was used as a background and subtracted from each subsequent scan.

XPS was performed using a Kratos Axis Ultra DLD spectrometer, which consists of a high performance Al K $\alpha$  monochromatic X-ray source (1486.6 eV) and a high resolution spherical mirror analyzer. Xray source was operated at 105 W and the emitted photoelectrons were collected at the analyzer entrance slit normal to the sample surface. The data acquisition was carried out in hybrid mode with analysis area of 700  $\times$  300  $\mu$ m. The survey spectra were recorded at pass energy of 160 eV with 0.5 eV step size and high resolution spectra were recorded at pass energy of 40 eV with step size of 0.1 eV. The pass energy 20 eV in the 700  $\times$  300  $\mu$ m analysis area is referred to the fwhm of 0.65 eV for Ag  $3d_{5/2}$ . The charge neutralizer with low energy electrons was used to exclude the surface charging effects, and the binding energy of C 1s at 285 eV was used as the charge reference. Samples were mounted using double-sided Scotch brand tape attached to a silicon substrate. For pure PFOS, the solution was evaporated on the substrate. For solids, GAC or MOF samples saturated with PFOS solution were dried on the tape. XPS data was analyzed by CasaXPS software using Gaussian/Lorentzian (GL(30)) line shape and Shirley background correction. The percentages of individual elements detected were determined from the relative composition analysis of the peak areas of the bands on the basis of the relative peak areas and their corresponding sensitivity factors to provide relative compositions.

### ■ RESULTS AND DISCUSSION

It should be noted that the PFOS concentrations utilized in these experiments are relatively high as compared to realistic amounts found in aqueous environments globally (EPA health advisory limit set at 70 ng/L). However, the scope of this study focuses on probing the capture of PFOS, which requires higher sorbate concentrations to observe saturation limits experimentally. Moreover, these higher concentrations also help one to evaluate the performance of novel sorbents as compared to traditional ones to assess longevity and lifetime of sorbent use in practical conditions. Consequently, we acknowledge that, under these experimental conditions, the PFOS species will likely aggregate to form micelles based on previously reported critical micelle concentrations (CMC) values. This would therefore affect the mechanism of sorption experimentally

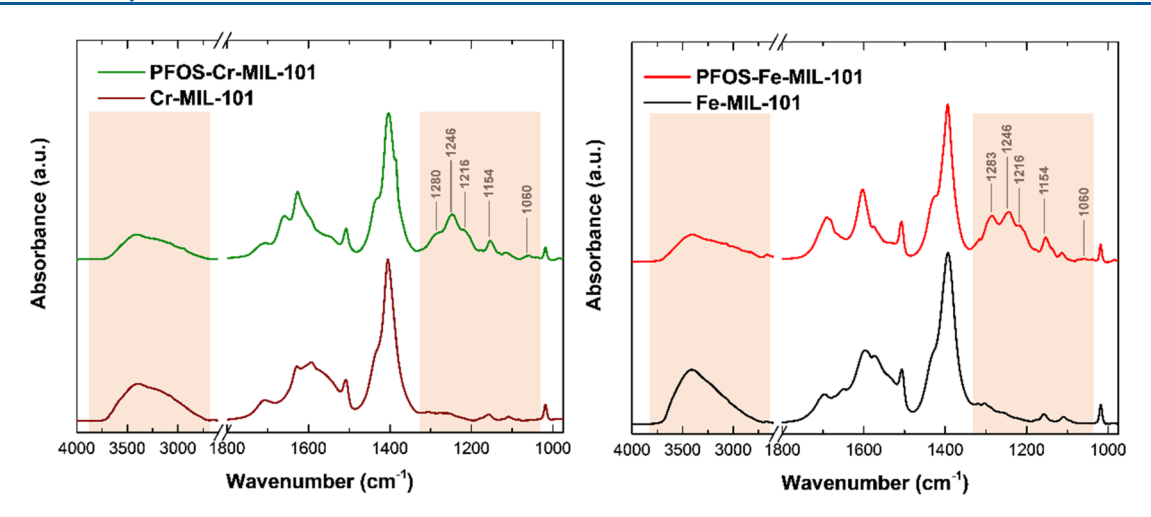


Figure 3. Infrared spectra of Cr-MIL-101 and Fe-MIL-101 before and after exposure to 10 mM PFOS (after drying).

observed in our studies, compared to mechanisms that may occur at much lower PFOS concentrations. For this reason, the intent of sorption characterization in this work is to probe the molecular interactions that we expect to occur. Given the presence of micelles with exposed polar head groups containing the sulfonic acid moiety, characterization of sorption affinity is expected to reveal significant sulfur (from sorbate) to framework interactions.

In order to quantify and understand sorption affinities, the supernatants of PFOS solutions containing both Cr-MIL-101 and Fe-MIL-101 were interrogated using <sup>19</sup>F liquid-state NMR. The raw time dependent <sup>19</sup>F NMR spectra showing the observed fluorine resonance is shown in Figure S2. However, the reduction in the peak intensity of the resonance at –79 ppm over time is assumed to represent the general depletion of PFOS from the supernatant bulk phase over time. <sup>51</sup> Subsequently, this decay profile is assumed to directly correspond to the amount of PFOS sorbed onto the MOF. As observed in Figure 2, there is clearly a decay of the mobile, bulk phase PFOS concentrations in the solutions in contact with either Cr-MIL-101 or Fe-MIL-101 (Figure 2, parts a and b, respectively) due to their sorption and immobilization.

Closer analysis of the data in Figure 2 shows that the peak intensity decreases rapidly in the early stage (within 2 h) of sorption and plateaus after longer sorption times ( $\sim$ 40 h). To quantify and distinguish the performance between the materials, the sorption profiles were fitted to a double exponential decay function (eq S1). In comparing the fitted time constants (Table S1), it is clear that Cr-MIL-101 adsorbs PFOS  $\sim$  2 times faster than Fe-MIL-101. An extrapolation of the fitted curves shows that maximum removal of PFOS from the bulk phase supernatant solution can be estimated to take nearly 250 h for Fe-MIL-101 while it takes only  $\sim$ 125 h for Cr-MIL-101. Also Cr-MIL-101 is observed to be superior to Fe-MIL-101 in the sorption of PFOS at the early stage of sorption ( $A_1 > A_2$ ; see Table S1).

Similarly, as a control, GAC was also probed for PFOS sorption using liquid state  $^{19}$ F NMR, and the signal intensities were tracked over time. Surprisingly, at this concentration, the intensity of the resonance at -79 ppm was observed to stay largely invariant in the course of  $\sim 15$  h as shown in Figure 2c, indicating little or no change in the bulk phase PFOS concentration in contact with activated carbon the sorbent. From this result, it can be inferred that PFOS sorption with

carbon is poor, and it further emphasizes the remarkable uptake observed by these highly porous MOF materials. It can also be concluded that the sorption capacity for PFOS by MIL-101 is far superior compared to the chosen GAC sorbent.

After observation of a clear indication of PFOS sorption by these MOFs, postsorption analysis of these materials was performed to gain insight into sorbate—sorbent interactions. First, the dried sorbent post removal of PFOS contact solution was subjected to <sup>19</sup>F solid-state NMR (Figure S3). The solid-state <sup>19</sup>F NMR spectrum clearly indicates the presence of adsorbed PFOS on the sorbents. For comparison, pristine MOFs (pre-PFOS exposure) were also subjected to the solid state NMR studies where no <sup>19</sup>F resonances are observed, as expected in a sample devoid of fluorine. Therefore, taken together, the progressive decrease of <sup>19</sup>F resonance intensity of PFOS solutions in contact with MOFs observed by liquid NMR spectra and the clear evidence of sorbed PFOS onto the MOFs revealed by <sup>19</sup>F solid-state NMR indicate that PFOS is captured from solution onto the MOFs.

To probe changes in the sorbent structure after sorption via vibrational frequencies and verify the presence of PFOS in the MOF frameworks, infrared spectroscopy was also utilized. The transmission IR spectra of pristine MOFs as well as MOFs post PFOS exposure are shown in Figure 3. The summary of the assignments of the main IR bands is listed in Table S2. For ease of comparison, bands in three separate regions were considered, i.e., 3600-3000 cm<sup>-1</sup> for -OH vibration, 1700-1300 cm<sup>-1</sup> for the assignments from aromatic ring or carboxylate of the pristine MIL-101 MOFs, and 1300-1050 cm<sup>-1</sup> for the functional groups from the PFOS. The most striking difference for the pristine MOFs and MOFs post PFOS exposure are the appearance of several new peaks at 1280, 1246, 1216, 1154, and 1060 cm<sup>-1</sup>, which are assigned to the  $-CF_2$ ,  $-CF_3$ , or  $-SO_3^-$  functional groups, respectively. These peaks are slightly shifted compared to those previously reported in the literature. 52,53 This might be due to the confinement of PFOS molecules within the pores of these MOFs.<sup>54</sup> We also note that the intensity of the broad band at 3600-3000 cm<sup>-1</sup> is clearly decreased with the addition of PFOS. This band is formed by the -OH stretching of H<sub>2</sub>O molecules stabilized in the pores of the MOFs via hydrogen bond.<sup>43</sup> It further supports that PFOS are loaded into the cages of MIL-101. In addition, we also note that the bands in the region of  $1700-1300 \text{ cm}^{-1}$ , assigned to the -C=C or -OCO

groups from the pristine MIL-101, are largely retained after the sorption of PFOS, which is indicative of a stable MOF structure. 55,56

To further understand the interaction between the PFOS and MIL framework, XPS was conducted on both Cr-MIL-101 and Fe-MIL-101 before and after PFOS exposure (Figure 4).

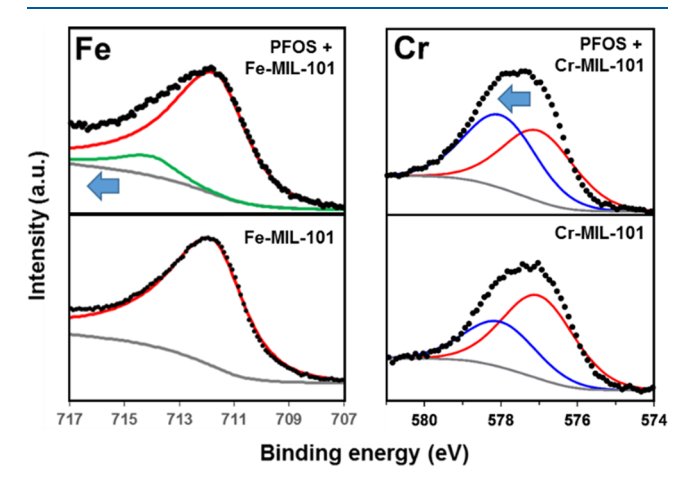


**Figure 4.** X-ray photoelectron spectra showing changes in binding energies (arrows) of the metal node of the MOF framework for both Cr-MIL-101 and Fe-MIL-101 before and after exposure to PFOS. For simplicity, only Fe  $2p_{3/2}$  and Cr  $2p_{3/2}$  portions of the spectra are shown here.

This is mainly to see if any changes in electron density occurred on the key elements involved in the capture process, and if it can throw any insight into the element specific affinities. For Cr-MIL-101, the Cr region of the photoelectron spectrum of the pristine sample shows two Cr environments as demonstrated by the Cr 2p<sub>3/2</sub> region being resolved into two species with binding energy values of 577.1 and 578.2 eV respectively, with the lower oxidation state being the dominant contributor. MOF exposure to PFOS resulted in the higher Cr oxidation state gaining in intensity at the expense of the lower oxidation state, suggesting chromium oxidation in the presence of PFOS (Figure 4). It should be noted that a detectable change in the Cr binding energies upon sorption is in itself quite significant since the relative abundance of Cr from the MOF framework compared to PFOS molecules adsorbed is so large. This alone suggests strong sorption affinities of PFOS on the MOF. For Fe-MIL-101, the magnitude of this change, as compared to Cr, is smaller. The Fe is observed to get oxidized, with the binding energy maxima of the Fe 2p<sub>3/2</sub> line changing from 711.8 eV in the pre-exposed sample to 712.1 eV in the sample post PFOS exposure. Compared to Cr-MIL-101, based on metal node binding energies alone, the affinity for PFOS on Fe-MIL-101 is seemingly less as shown in Figure 4.

Accordingly, the F region of the XPS spectrum (Figure 5) of PFOS loaded MOFs shows an opposite shift, as expected. The F of PFOS shows a single 1s line at 689.3 eV, while the spectrum of PFOS sorbed onto Cr-MIL-101 showed an additional second F environment with lower binding energy of 688.5 eV suggesting the F center gaining electron density. Interestingly, a similar, yet more pronounced reduction of the F atoms is observed for Fe-MIL-101. In both cases, this reduction is suggestive of a synergistic redox process with the F atoms pulling electrons away from the metal center and thereby getting reduced. On the basis of the fluorine spectrum

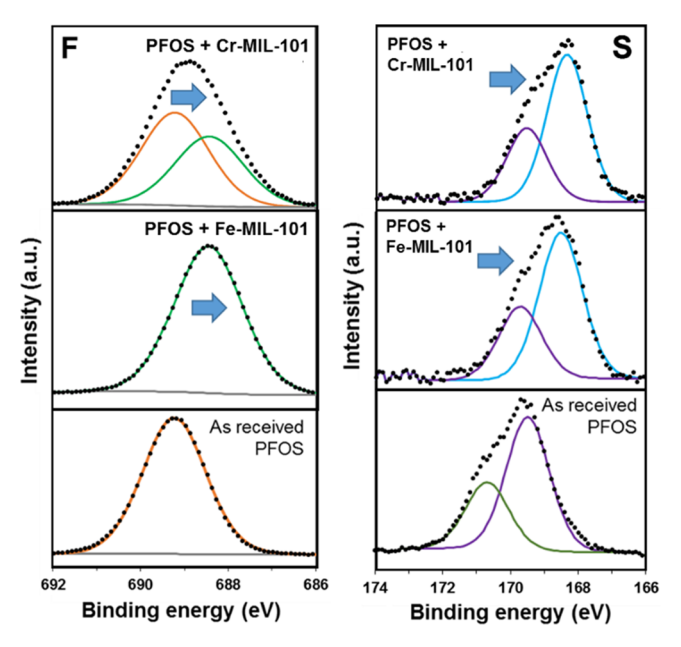


**Figure 5.** X-ray photoelectron spectra showing changes in binding energies (arrows) of the fluorine atoms (F 1s) from the hydrophobic tail and the sulfur atom (S 2p) from the polar headgroup for both Cr-MIL-101 and Fe-MIL-101 before and after exposure to PFOS.

alone, PFOS-exposed-Fe-MIL-101 has a more reduced F environment, suggesting stronger interactions with the fluorinated hydrophobic tail compared to those with Cr-MIL-101. Ultimately, the S region of the photoelectron spectrum must be probed since high concentrations of PFOS (past the CMC) are expected to have more sulfur-containing moieties exposed to sorption sites. This S 2p region of the spectrum shows a similar shift in the same direction as the F 1s spectrum, albeit the magnitude of the shift is significantly larger. This observation confirms the expectation that the sulfur containing head groups would be forced to interact more with sorption sites of the MOF frameworks compared with the hydrophobic tails. The  $2p_{3/2}$  sulfur line shifts from 169.5 eV in the PFOS sample to 168.3 eV in the PFOS-sorbed Cr-MIL-101 sample and to 168.8 eV in the PFOS-sorbed Fe-MIL-101 sample. This clear shift is indicative of a significantly reduced S environment after sorption compared to free PFOS. This also suggests a slightly stronger interaction with Cr-MIL-101 compared to Fe-MIL-101. Overall, considering the full photoelectron spectrum shift before and after PFOS exposure, it is speculated that given (1) the larger observed reduction in S environment, (2) the known enhanced exposure of sulfur moieties due to concentrations higher than the CMC and (3) increased observed oxidation in framework metal centers, and (4) the stronger Lewis acid sites that Cr-MIL-101 likely has a more favorable interaction with PFOS under these experimental conditions. It should also be noted that the structural integrity and morphology of Cr-MIL-101 before and after exposure to PFOS was intact as shown by the PXRD, porosimetry, and microscopy studies (Figures S4-S7).

# CONCLUSIONS

We were able to probe both Cr-MIL-101 and Fe-MIL-101 for PFOS sorption using a number of experimental characterization techniques. In situ <sup>19</sup>F NMR experiments revealed faster kinetics for Cr-MIL-101 obtained with a relatively concentrated 10 mM solution of PFOS, while curve fitting

estimates revealed maximum capture to occur twice as fast as for Fe-MIL-101. Importantly, both MOFs significantly outperformed the traditionally used activated carbon sorbent, which showed little to no sorption of PFOS at these concentrations. Structural characterization of the MOFs before and after exposure of PFOS showed evidence of PFOS moieties from the IR spectra at 1300–1050 cm<sup>-1</sup>. Finally, analysis of the PFOS sorption affinity using XPS showed a stronger interaction to Cr-MIL-101 compared to Fe-MIL-101 due to a larger shift in binding energies of the metal node and sulfur moieties, which were expected to have significantly more interactions at this PFOS concentration versus the nonpolar fluorinated tail. Further research into the targeted capture of many other such perfluoroalkyl substances using similar MOF materials is ongoing.

#### ASSOCIATED CONTENT

# **S** Supporting Information

The Supporting Information is available free of charge on the ACS Publications website at DOI: 10.1021/acs.inorg-chem.9b00380.

Additional experimental details, NMR spectra and analysis, IR peak identification, PXRD, porosimetry, and microscopy results (PDF)

#### AUTHOR INFORMATION

#### **Corresponding Authors**

\*(S.C.) E-mail: Sayandev.Chatterjee@pnnl.gov. \*(R.K.M.) E-mail: Radhakishan.Motkuri@pnnl.gov.

#### ORCID 6

Dushyant Barpaga: 0000-0003-2271-6213 Jian Zheng: 0000-0003-2054-9482 Kee Sung Han: 0000-0002-3535-1818 Jennifer A. Soltis: 0000-0002-7442-0193

Vaithiyalingam Shutthanandan: 0000-0003-2957-7535

Sayandev Chatterjee: 0000-0003-2218-5635 Radha Kishan Motkuri: 0000-0002-2079-4798

# Notes

The authors declare no competing financial interest.

# ACKNOWLEDGMENTS

This research was supported by the "Laboratory Directed Research and Development Program at the Pacific Northwest National Laboratory (SEED EED)". We also acknowledge the U.S. Department of Energy (DOE)'s Geothermal Technologies Office (GTO) for MOF materials development. S.B. acknowledges the support from National Science Foundation (NSF) grant, 1751759, CAREER. Part of this research was performed at Environmental Molecular Sciences Laboratory, a national scientific user facility at Pacific Northwest National Laboratory (PNNL) managed by the Department of Energy's Office of Biological and Environmental Research. PNNL is operated by Battelle for the U.S. Department of Energy under Contract DE-AC05-76RL01830.

#### REFERENCES

- (1) Lindstrom, A. B.; Strynar, M. J.; Libelo, E. L. Polyfluorinated Compounds: Past, Present, and Future. *Environ. Sci. Technol.* **2011**, 45, 7954–7961.
- (2) Houtz, E.; Wang, M. M.; Park, J. S. Identification and Fate of Aqueous Film Forming Foam Derived Per- and Polyfluoroalkyl

Substances in a Wastewater Treatment Plant. Environ. Sci. Technol. 2018, 52, 13212-13221.

- (3) Post, G. B.; Cohn, P. D.; Cooper, K. R. Perfluorooctanoic acid (PFOA), an emerging drinking water contaminant: A critical review of recent literature. *Environ. Res.* **2012**, *116*, 93–117.
- (4) Hu, X. D. C.; Andrews, D. Q.; Lindstrom, A. B.; Bruton, T. A.; Schaider, L. A.; Grandjean, P.; Lohmann, R.; Carignan, C. C.; Blum, A.; Balan, S. A.; Higgins, C. P.; Sunderland, E. M. Detection of Polyand Perfluoroalkyl Substances (PFASs) in US Drinking Water Linked to Industrial Sites, Military Fire Training Areas, and Wastewater Treatment Plants. *Environ. Sci. Technol. Lett.* **2016**, *3*, 344–350.
- (5) Ducatman, A.; Zhang, J. J.; Fan, H. M. Prostate-Specific Antigen and Perfluoroalkyl Acids in the C8 Health Study Population. *J. Occup. Environ. Med.* **2015**, *57*, 111–114.
- (6) Olsen, G. W.; Hansen, K. J.; Stevenson, L. A.; Burris, J. M.; Mandel, J. H. Human donor liver and serum concentrations of perfluoroctanesulfonate and other perfluorochemicals. *Environ. Sci. Technol.* **2003**, *37*, 888–891.
- (7) Kennedy, G. L.; Butenhoff, J. L.; Olsen, G. W.; O'Connor, J. C.; Seacat, A. M.; Perkins, R. G.; Biegel, L. B.; Murphy, S. R.; Farrar, D. G. The toxicology of perfluorooctanoate. *Crit. Rev. Toxicol.* **2004**, *34*, 351–384.
- (8) Merino, N.; Qu, Y.; Deeb, R. A.; Hawley, E. L.; Hoffmann, M. R.; Mahendra, S. Degradation and Removal Methods for Perfluoroalkyl and Polyfluoroalkyl Substances in Water. *Environ. Eng. Sci.* **2016**, 33, 615–649.
- (9) Rahman, M. F.; Peldszus, S.; Anderson, W. B. Behaviour and fate of perfluoroalkyl and polyfluoroalkyl substances (PFASs) in drinking water treatment: A review. *Water Res.* **2014**, *50*, 318–340.
- (10) Hamid, H.; Li, L. Y.; Grace, J. R. Review of the fate and transformation of per- and polyfluoroalkyl substances (PFASs) in landfills. *Environ. Pollut.* **2018**, 235, 74–84.
- (11) Chularueangaksorn, P.; Tanaka, S.; Fujii, S.; Kunacheva, C. Batch and Column Adsorption of Perfluorooctane Sulfonate on Anion Exchange Resins and Granular Activated Carbon. *J. Appl. Polym. Sci.* **2014**, *131*, 39782.
- (12) Ochoa-Herrera, V.; Sierra-Alvarez, R. Removal of perfluorinated surfactants by sorption onto granular activated carbon, zeolite and sludge. *Chemosphere* **2008**, 72, 1588–1593.
- (13) Schroder, H. F.; Jose, H. J.; Gebhardt, W.; Moreira, R. F. P. M.; Pinnekamp, J. Biological wastewater treatment followed by physicochemical treatment for the removal of fluorinated surfactants. *Water Sci. Technol.* **2010**, *61*, 3208–3215.
- (14) Ji, W.; Xiao, L. L.; Ling, Y. H.; Ching, C.; Matsumoto, M.; Bisbey, R. P.; Helbling, D. E.; Dichtel, W. R. Removal of GenX and Perfluorinated Alkyl Substances from Water by Amine-Functionalized Covalent Organic Frameworks. *J. Am. Chem. Soc.* **2018**, *140*, 12677—12681.
- (15) Das, A. K.; Vemuri, R. S.; Kutnyakov, I.; Mc Grail, B. P.; Motkuri, R. K. An Efficient Synthesis Strategy for Metal-Organic Frameworks: Dry-Gel Synthesis of MOF-74 Framework with High Yield and Improved Performance. Sci. Rep. 2016, 6, 28050.
- (16) Islamoglu, T.; Ray, D.; Li, P.; Majewski, M. B.; Akpinar, I.; Zhang, X.; Cramer, C. J.; Gagliardi, L.; Farha, O. K. From Transition Metals to Lanthanides to Actinides: Metal-Mediated Tuning of Electronic Properties of Isostructural Metal-Organic Frameworks. *Inorg. Chem.* 2018, 57, 13246–13251.
- (17) Nandi, S.; Maity, R.; Chakraborty, D.; Ballav, H.; Vaidhyanathan, R. Preferential Adsorption of CO2 in an Ultramicroporous MOF with Cavities Lined by Basic Groups and Open-Metal Sites. *Inorg. Chem.* **2018**, *57*, 5267–5272.
- (18) Liu, J.; Zheng, J.; Barpaga, D.; Sabale, S.; Arey, B.; Derewinski, M. A.; McGrail, B. P.; Motkuri, R. K. A Tunable Bimetallic MOF-74 for Adsorption Chiller Applications. *Eur. J. Inorg. Chem.* **2018**, 2018, 885–889.
- (19) Pal, A.; Chand, S.; Das, M. C. A Water-Stable Twofold Interpenetrating Microporous MOF for Selective CO2 Adsorption and Separation. *Inorg. Chem.* **2017**, *56*, 13991–13997.

(20) Thallapally, P. K.; Tian, J.; Kishan, M. R.; Fernandez, C. A.; Dalgarno, S. J.; McGrail, P. B.; Warren, J. E.; Atwood, J. L. Flexible (Breathing) Interpenetrated Metal-Organic Frameworks for CO2 Separation Applications. J. Am. Chem. Soc. 2008, 130, 16842.

- (21) Kishan, M. R.; Tian, J.; Thallapally, P. K.; Fernandez, C. A.; Dalgarno, S. J.; Warren, J. E.; McGrail, B. P.; Atwood, J. L. Flexible metal-organic supramolecular isomers for gas separation. *Chem. Commun.* **2010**, *46*, 538–540.
- (22) Morris, W.; Volosskiy, B.; Demir, S.; Gandara, F.; McGrier, P. L.; Furukawa, H.; Cascio, D.; Stoddart, J. F.; Yaghi, O. M. Synthesis, Structure, and Metalation of Two New Highly Porous Zirconium Metal-Organic Frameworks. *Inorg. Chem.* **2012**, *51*, 6443–6445.
- (23) Motkuri, R. K.; Thallapally, P. K.; Annapureddy, H. V. R.; Dang, L. X.; Krishna, R.; Nune, S. K.; Fernandez, C. A.; Liu, J.; McGrail, B. P. Separation of polar compounds using a flexible metalorganic framework. *Chem. Commun.* **2015**, *51*, 8421–8424.
- (24) Kang, Y. S.; Lu, Y.; Chen, K.; Zhao, Y.; Wang, P.; Sun, W. Y. Metal-organic frameworks with catalytic centers: From synthesis to catalytic application. *Coord. Chem. Rev.* **2019**, *378*, 262–280.
- (25) Hou, S. L.; Dong, J.; Jiang, X. L.; Jiao, Z. H.; Zhao, B. A Noble-Metal-Free Metal-Organic Framework (MOF) Catalyst for the Highly Efficient Conversion of CO2 with Propargylic Alcohols. *Angew. Chem., Int. Ed.* **2019**, *58*, 577–581.
- (26) Huang, N.; Drake, H.; Li, J. L.; Pang, J. D.; Wang, Y.; Yuan, S.; Wang, Q.; Cai, P. Y.; Qin, J. S.; Zhou, H. C. Flexible and Hierarchical Metal-Organic Framework Composites for High-Performance Catalysis. *Angew. Chem., Int. Ed.* **2018**, *57*, 8916–8920.
- (27) Lei, X. J.; Hou, X. Y.; Li, S. N.; Jiang, Y. C.; Sun, G. X.; Hu, M. C.; Zhai, Q. G. Design of High-Symmetrical Magnesium-Organic Frameworks with Acetate as Modulator and Their Fluorescence Sensing Performance. *Inorg. Chem.* **2018**, *57*, 14280–14289.
- (28) Liu, R. L.; Liu, Y. R.; Yu, S. H.; Yang, C. L.; Li, Z. F.; Li, G. A Highly Proton-Conductive 3D Ionic Cadmium-Organic Framework for Ammonia and Amines Impedance Sensing. ACS Appl. Mater. Interfaces 2019, 11, 1713–1722.
- (29) Zhang, Y. M.; Yuan, S.; Day, G.; Wang, X.; Yang, X. Y.; Zhou, H. C. Luminescent sensors based on metal-organic frameworks. *Coord. Chem. Rev.* **2018**, 354, 28–45.
- (30) Levitskaia, T. G.; Chatterjee, S.; Pence, N. K.; Romero, J.; Varga, T.; Engelhard, M. H.; Du, Y. G.; Kovarik, L.; Arey, B. W.; Bowden, M. E.; Walter, E. D. Inorganic tin aluminophosphate nanocomposite for reductive separation of pertechnetate. *Environ. Sci.: Nano* **2016**, *3*, 1003–1013.
- (31) Chatterjee, S.; Norton, A. E.; Edwards, M. K.; Peterson, J. M.; Taylor, S. D.; Bryan, S. A.; Andersen, A.; Govind, N.; Albrecht-Schmitt, T. E.; Connick, W. B.; Levitskaia, T. G. Highly Selective Colorimetric and Luminescence Response of a Square-Planar Platinum(II) Terpyridyl Complex to Aqueous TcO4-. *Inorg. Chem.* 2015, 54, 9914–9923.
- (32) Hasan, Z.; Jhung, S. H. Removal of hazardous organics from water using metal-organic frameworks (MOFs): Plausible mechanisms for selective adsorptions. *J. Hazard. Mater.* **2015**, 283, 329–339.
- (33) Dhaka, S.; Kumar, R.; Deep, A.; Kurade, M. B.; Ji, S. W.; Jeon, B. H. Metal-organic frameworks (MOFs) for the removal of emerging contaminants from aquatic environments. *Coord. Chem. Rev.* **2019**, 380, 330–352.
- (34) Chatterjee, S.; Del Negro, A. S.; Edwards, M. K.; Bryan, S. A.; Kaval, N.; Pantelic, N.; Morris, L. K.; Heineman, W. R.; Seliskar, C. J. Luminescence-Based Spectroelectrochemical Sensor for [Tc(dmpe) (3)](2+/+) (dmpe = 1,2-bis(dimethylphosphino)ethane) within a Charge-Selective Polymer Film. *Anal. Chem.* **2011**, 83, 1766–1772.
- (35) Chatterjee, S.; Fujimoto, M. S.; Cheng, Y. H.; Kargupta, R.; Soltis, J. A.; Motkuri, R. K.; Basuray, S. Improving the Sensitivity of Electrochemical Impedance Sensors through a Complementary Luminescent Mode: A New Spectroelectrochemical Approach. *Sens. Actuators, B* **2019**, 284, 663–674.
- (36) Sini, K.; Bourgeois, D.; Idouhar, M.; Carboni, M.; Meyer, D. Metal-organic framework sorbents for the removal of perfluorinated

compounds in an aqueous environment. New J. Chem. 2018, 42, 17889-17894.

- (37) Liu, K.; Zhang, S. Y.; Hu, X. Y.; Zhang, K. Y.; Roy, A.; Yu, G. Understanding the Adsorption of PFOA on MIL-101(Cr)-Based Anionic-Exchange Metal-Organic Frameworks: Comparing DFT Calculations with Aqueous Sorption Experiments. *Environ. Sci. Technol.* **2015**, *49*, 8657–8665.
- (38) Chen, M. J.; Yang, A. C.; Wang, N. H.; Chiu, H. C.; Li, Y. L.; Kang, D. Y.; Lo, S. L. Influence of crystal topology and interior surface functionality of metal-organic frameworks on PFOA sorption performance. *Microporous Mesoporous Mater.* **2016**, 236, 202–210.
- (39) Li, Y. X.; Yang, Z. X.; Wang, Y. L.; Bai, Z. L.; Zheng, T.; Dai, X.; Liu, S. T.; Gui, D. X.; Liu, W.; Chen, M.; Chen, L. H.; Diwu, J.; Zhu, L. Y.; Zhou, R. H.; Chai, Z. F.; Albrecht-Schmitt, T. E.; Wang, S. A mesoporous cationic thorium-organic framework that rapidly traps anionic persistent organic pollutants. *Nat. Commun.* 2017, 8, 1354.
- (40) Karimian, N.; Stortini, A. M.; Moretto, L. M.; Costantino, C.; Bogialli, S.; Ugo, P. Electrochemosensor for Trace Analysis of Perfluorooctanesulfonate in Water Based on a Molecularly Imprinted Poly(o-phenylenediamine) Polymer. *Acs Sensors* **2018**, *3*, 1291–1298.
- (41) Scott, B. F.; Moody, C. A.; Spencer, C.; Small, J. M.; Muir, D. C. G.; Mabury, S. A. Analysis for perfluorocarboxylic acids/anions in surface waters and precipitation using GC-MS and analysis of PFOA from large-volume samples. *Environ. Sci. Technol.* **2006**, *40*, 6405–6410.
- (42) Motkuri, R. K.; Annapureddy, H. V. R.; Vijaykumar, M.; Schaef, H. T.; Martin, P. F.; McGrail, B. P.; Dang, L. X.; Krishna, R.; Thallapally, P. K. Fluorocarbon adsorption in hierarchical porous frameworks. *Nat. Commun.* **2014**, *5*, 4368.
- (43) Zheng, J.; Vemuri, R. S.; Estevez, L.; Koech, P. K.; Varga, T.; Camaioni, D. M.; Blake, T. A.; McGrail, B. P.; Motkuri, R. K. Pore-Engineered Metal-Organic Frameworks with Excellent Adsorption of Water and Fluorocarbon Refrigerant for Cooling Applications. *J. Am. Chem. Soc.* **2017**, *139*, 10601–10604.
- (44) Zheng, J.; Barpaga, D.; Gutierrez, O. Y.; Browning, N. D.; Mehdi, B. L.; Farha, O. K.; Lercher, J. A.; McGrail, B. P.; Motkuri, R. K. Exceptional Fluorocarbon Uptake with Mesoporous Metal—Organic Frameworks for Adsorption-Based Cooling Systems. *ACS Applied Energy Materials* **2018**, *1*, 5853—5858.
- (45) Jun, J. W.; Tong, M. M.; Jung, B. K.; Hasan, Z.; Zhong, C. L.; Jhung, S. H. Effect of Central Metal Ions of Analogous Metal-Organic Frameworks on Adsorption of Organoarsenic Compounds from Water: Plausible Mechanism of Adsorption and Water Purification. *Chem. Eur. J.* **2015**, *21*, 347–354.
- (46) Latroche, M.; Surble, S.; Serre, C.; Mellot-Draznieks, C.; Llewellyn, P. L.; Lee, J. H.; Chang, J. S.; Jhung, S. H.; Ferey, G. Hydrogen storage in the giant-pore metal-organic frameworks MIL-100 and MIL-101. *Angew. Chem., Int. Ed.* **2006**, *45*, 8227–8231.
- (47) Ferey, G.; Mellot-Draznieks, C.; Serre, C.; Millange, F.; Dutour, J.; Surble, S.; Margiolaki, I. A chromium terephthalate-based solid with unusually large pore volumes and surface area. *Science* **2005**, *309*, 2040–2042.
- (48) Guo, Q.; Ren, L. M.; Kumar, P.; Cybulskis, V. J.; Mkhoyan, K. A.; Davis, M. E.; Tsapatsis, M. A Chromium Hydroxide/MIL-101(Cr) MOF Composite Catalyst and Its Use for the Selective Isomerization of Glucose to Fructose. *Angew. Chem., Int. Ed.* **2018**, *57*, 4926–4930.
- (49) Tang, J.; Yang, M.; Yang, M.; Wang, J. J.; Dong, W. J.; Wang, G. Heterogeneous Fe-MIL-101 catalysts for efficient one-pot four-component coupling synthesis of highly substituted pyrroles. *New J. Chem.* **2015**, *39*, 4919–4923.
- (50) Martin, J. W.; Mabury, S. A.; Solomon, K. R.; Muir, D. C. G. Bioconcentration and tissue distribution of perfluorinated acids in rainbow trout (Oncorhynchus mykiss). *Environ. Toxicol. Chem.* **2003**, 22, 196–204.
- (51) Wallace, M.; Iggo, J. A.; Adams, D. J. Using solution state NMR spectroscopy to probe NMR invisible gelators. *Soft Matter* **2015**, *11*, 7739–7747.

(52) Gao, X. D.; Chorover, J. Adsorption of perfluorooctanoic acid and perfluorooctanesulfonic acid to iron oxide surfaces as studied by flow-through ATR-FTIR spectroscopy. *Environ. Chem.* **2012**, *9*, 148–157.

- (53) Lin, H.; Wang, Y. J.; Niu, J. F.; Yue, Z. H.; Huang, Q. G. Efficient Sorption and Removal of Perfluoroalkyl Acids (PFAAs) from Aqueous Solution by Metal Hydroxides Generated in Situ by Electrocoagulation. *Environ. Sci. Technol.* **2015**, *49*, 10562–10569.
- (54) Tripathi, A. K.; Verma, Y. L.; Singh, R. K. Thermal, electrical and structural studies on ionic liquid confined in ordered mesoporous MCM-41. *J. Mater. Chem. A* **2015**, *3*, 23809–23820.
- (55) Zhang, Z. J.; Huang, S. S.; Xian, S. K.; Xi, H. X.; Li, Z. Adsorption Equilibrium and Kinetics of CO2 on Chromium Terephthalate MIL-101. *Energy Fuels* **2011**, 25, 835–842.
- (56) Liu, Q.; Ning, L. Q.; Zheng, S. D.; Tao, M. N.; Shi, Y.; He, Y. Adsorption of Carbon Dioxide by MIL-101(Cr): Regeneration Conditions and Influence of Flue Gas Contaminants. *Sci. Rep.* **2013**, 3, 3.
- (57) Kim, D. W.; Kim, H. G.; Cho, D. H. Catalytic performance of MIL-100 (Fe, Cr) and MIL-101 (Fe, Cr) in the isomerization of endo- to exo-dicyclopentadiene. *Catal. Commun.* **2016**, *73*, 69–73.